VACUUM LASER ACCELERATION TESTS*

Y. Liu†, P. He, D. Cline, University of California, Los Angeles, CA 90095-1547

Abstract

We propose to test for the possibility of accelerating an electron beam (utilizing the existing high-power CO_2 laser and low emittance electron beam at Brookhaven Accelerator Test Facility) in vacuum to the current CO_2 laser power limit. The latest vacuum laser acceleration results can be verified [1] by the schemes discussed here.

1 INTRODUCTION

Laser acceleration in vacuum has been studied theoretically for many years and several schemes utilizing focused Gaussian laser beam(s) have been proposed [2]–[9]. In most of the schemes, researchers attempt to confine the interaction to a finite length, but none of them has been successful until recently. In 1997, a group of physicists [1] demonstrated direct acceleration of free electrons in vacuum to MeV energies by a linearly polarized and intense subpicosecond laser pulse, appearing directly violate a long-held theorem [10].

A focused, radially polarized, Gaussian laser beam can produce a stronger longitudinal electric field than the linearly polarized one [11]–[14]. The Brookhaven Accelerator Test Facility (ATF) provides a radially polarized, high-power, Gaussian CO_2 laser beam (3-TW, 1-ps) [15, 16] and a high-quality electron beam [17] with which to perform the vacuum laser acceleration test. The electron energy modulation will be ramped up to the current CO_2 laser power limit. Moreover, since the Compton Scattering experiment [18] was recently conducted on the ATF beamline #1 (which is shared by the STELLA experiment), the hardware and optics configurations will require only slight modification since they are quite similar to the requirements for the vacuum acceleration experiment. This similarity provides a great opportunity to utilizing the existing hardware with little additional cost.

2 INTENSITY DISTRIBUTIONS OF A FOCUSED DONUT-SHAPED LASER BEAM

As seen in Figure 1, a parallel or weakly focused Gaussian laser beam passes through an axicon telescope (consisting of two thin axicon lenses) and is focused by a thin lens at distance F. The intensity distribution of the donut-shaped

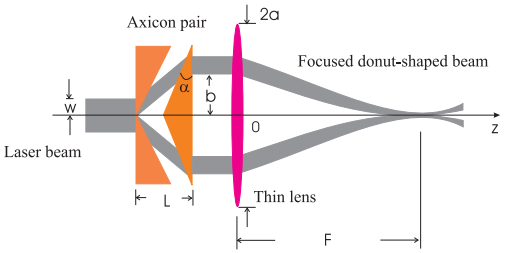

Figure 1: Schematic of generating and focusing a donut-shaped beam at the distance F by a pair of axicon lenses and a thin lens.

beam transformed from a Gaussian beam is expressed by

$$I(r_0) = \frac{P_0}{\pi w^2}\left(1 - \frac{b}{r_0}\right)\exp\left[-2\left(\frac{r_0 - b}{w}\right)^2\right], r_0 \geq b, \quad (1)$$

where P_0 is the peak power and $b = L\tan(\theta)$ is the inner radius of the donut-shaped beam, where L is the distance between two axicons and θ is the refraction angle of the axicon, and w is the beam radius at the first axicon surface. By adjusting L, the inner radius, b, is controllable. The maximum intensity, I_m, occurs at r_m where the differential of Eq. (1) is equal to zero. Note that Eq. (1) is derived ideally from the geometrical optics of the axicon telescope. The diffraction of the laser beam in the course of conversion is neglected.

Figure 2 shows the geometric configuration for the usual Fresnel–Kirchhoff diffraction integral formulation with aperture-plane integration. The field amplitude distribution at point $P(r,\theta)$ in the x′–y′ plane is given, up to a constant phase factor, by the Fresnel–Kirchhoff integral for an aperture radius a [19],

$$\Psi_p(r,\theta) = \frac{k}{z}\int \Psi_0(r_0,\theta_0)\exp(-ikR)\Phi_l dS, \quad (2)$$

where k is the wavenumber; $\Psi_0(r_0,\theta_0) \sim \sqrt{I(r_0)}$ is the field amplitude distribution at point $Q(r_0,\theta_0)$ of the lens surface and $I(r_0)$ is given by Eq. (1); Φ_l is the phase retar-

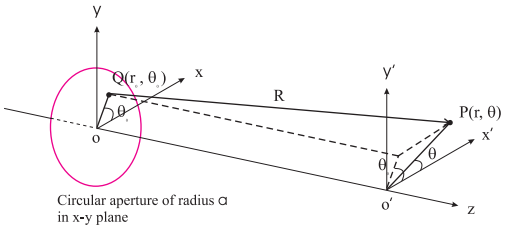

Figure 2: Geometry for Fresnel–Kirchhoff aperture-plane diffraction formulation.

* Work supported by U.S. Department of Energy, Grant No. DE-FG03-92ER40695 with UCLA

† Email: yliu@physics.ucla.edu

dation of the lens expressed as

$$\Phi_l = \exp\left(\frac{ikr_0^2}{2F}\right), \tag{3}$$

where F is the geometrical focal length; and R is the distance between Q and P,

$$R \approx z + \frac{r_0^2 + r^2 - 2r_0 r\cos(\theta_0 - \theta)}{2z}, \tag{4}$$

Substituting Eqs. (1), (3), and (4) into Eq. (2)

$$\begin{aligned}\Psi_p(r,\theta) &= E_0\frac{k}{z}\int_b^a \left(1-\frac{b}{r_0}\right)^{1/2}\exp\left[-\frac{1}{2}\left(\frac{r_0-b}{w}\right)^2\right] \\ &\times \exp\left[ik\left(\frac{r_0^2}{2F} - z - \frac{r_0 2 + r^2}{2z}\right)\right] \\ &\times J_0\left(\frac{kr_0 r}{z}\right) r_0 dr_0 d\theta_0,\end{aligned} \tag{5}$$

where E_0 is a constant. The relation $\int_0^{2\pi}\exp[ix\cos(\theta_0 - \theta)] = 2\pi J_0(x)$ was used to get Eq. (5), the numerical results of which are shown in Figure 3. Where the lens aperture radius is $a = 2.5$ cm and focal length is $F = 15.0$ cm, the inner radius of the donut-shaped beam is $b = 1.0$ cm and the width is $w = 0.5$ cm at the lens surface. The small peaks at $r = 0$ in Figure 3(a), (b), and (d) are from diffraction effect. The beam width at the focal plane is $w_0 = 31\,\mu$m [Figure 3(c)] and the donut feature vanishes (w_0 is defined as the beam radius where the intensity drops to e^{-2}). Figure 4 shows the laser intensity distribution on the beam z-axis.

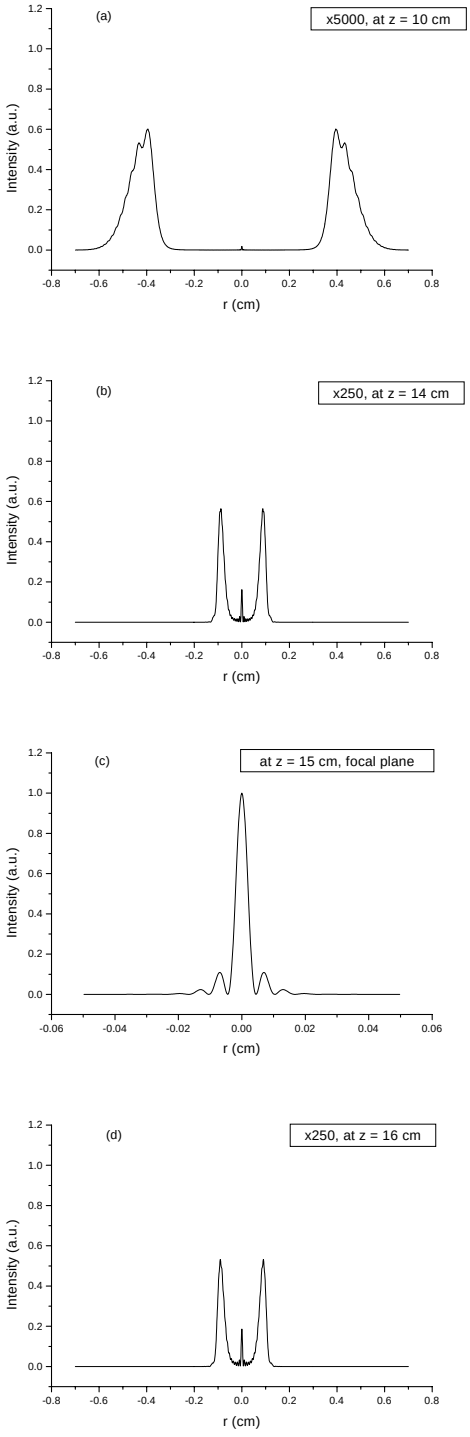

Figure 3: Cross sections of the focused donut beam intensity distributions in different planes. The focal lens position is at z = 0. Note, different scales for r-axes and the intensities in (a), (b) and (d) are normalized by (c).

3 CONCEPTUAL DESIGN OF THE EXPERIMENT

The proposed experiment is to perform four laser–electron beam-interaction processes. The conceptual schematic of the first two test processes is shown in Figure 5. In the first process, a linearly polarized, axisymmetric, annular ("donut-shaped") Gaussian-distributed, CO_2 laser beam is delivered to a vacuum chamber through a ZnSe window. A parabolic mirror with a hole is positioned along the electron beam path (z-axis) in the chamber. The hole is located at the mirror optical center and allows the electron beam to meet with the laser beam in the focal region. A pop-in target, located near the focal point, is able to travel along the beam axis. This diagnostic device is used to align the laser beam with the electron beam in the focal region. The second process will repeat the first one [20], but will utilize a radially polarized beam, which will be delivered by the existing radially polarized converter built for the STELLA experiment. The third process will perform a scheme with two crossed beams, as shown in Figure 6. The two beams are split from a single beam by a beamsplitter and have a phase difference π in the interaction region. The last is a single beam scheme, where one laser beam and the electron beam will cross at the laser focal point with small angle (one of the laser beams having been turned off, see Figure 6).

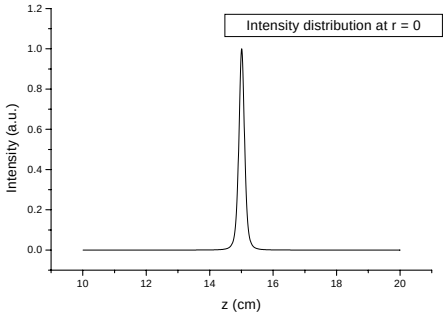

Figure 4: Laser intensity distribution along the beam (z) axis at r = 0.

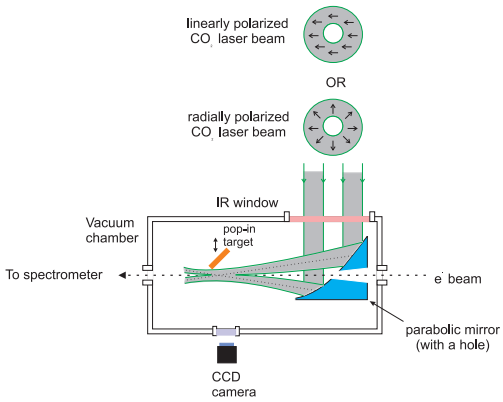

Figure 5: Conceptual layout of vacuum laser acceleration using donut-shaped beam.

4 DISCUSSIONS

The optics configuration, which is fairly simple, can be used to perform all four schemes with only slight changes of the optics setup outside the chamber. The scheme using a donut-shaped beam is able to overcome optical damage difficulty as laser power increases [20]. However, the interaction length is many times more than the Rayleigh length due to diffraction and will degrade or wash out the net energy gain according to the theorem [10]; however, the results reported in Ref. [1] will be verified eventually.

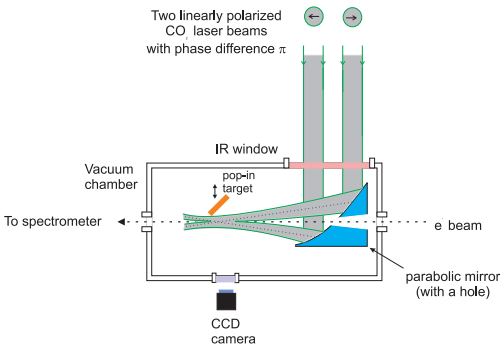

Figure 6: Conceptual layout of vacuum laser acceleration using a two crossed laser-beam scheme. If one of two beams is turned off, it becomes a single beam scheme.

5 REFERENCES

[1] G. Malka, E. Lefebvre, and J.L. Miquel, *Phys. Rev. Letts.*, **78** (17), 3314 (1997).

[2] M. O. Scully, *Appl. Phys. B*, **51**, 238 (1990).

[3] E.J. Bochove, G.T. Moore, and M.O. Scully, *Phys. Rev. A*, **46** (10), 6640 (1992).

[4] S. Takeuchi, R. Sugihara, and K. Shimoda, *J. Phys. Soci. Japan*, **63** (3), 1186 (1994).

[5] T. Hauser, W. Scheid, and H. Hora, *Phys. Lett. A*, **186**, 189 (1994).

[6] E. Esarey, P. Sprangle, and J. Krall, *Phys. Rev. E*, **52** (5), 5443 (1995).

[7] P. Sprangle, E. Esarey, J. Krall, and A. Ting, *Optics Comm.*, **124**, 69 (1996).

[8] B. Hafizi, E. Esarey, and P. Sprangle, *Phys. Rev. E*, **55** (3), 3539 (1997).

[9] B. Hafizi, A Ting, E. Esarey, P. Sprangle, and J. Knall, *Phys. Rev. E*, **55** (5), 5924 (1997).

[10] J.D. Lawson, *IEEE Trans. Nucl. Sic.* **NS-26**, 4217 (1979); P.M. Woodward, *J. Inst. Electr. Eng.* **93**, 1554 (1947); R.B. Palmer, *Lecture Notes in Physics 296, Frontiers of Particle Beams* (Springer, Berlin, 1988) p. 607.

[11] M. Lax, *Phys. Rev. A*, **11** (4), 1365 (1975).

[12] L. Cicchitelli, H. Hora, and R. Postle, *Phys. Rev. A*, **41** (7), 3727 (1990).

[13] K. Shimoda, *J. Phys. Soci. Japan*, **60** (1), 141 (1991).

[14] P.W. Milonni and J.H. Eberly, *Laser* (Wiley, New York, 1988), chap. 14; A. Yariv, *Quantum Electronics*, 3rd ed. (Wiley, New York, 1989), chap. 6.

[15] I. V. Pogorelsky, I. Ben-Zvi, J. Skaritka, et al., *AIP Conference Proceedings* **398** (1997) p. 937.

[16] ATF terawatt CO_2 laser specifications.

[17] D.T. Palmer, X.J. Wang, et al., *AIP Conference Proceedings* **398** (1997) p. 695.

[18] A.Tsunemi, A.Endo, et al., "Ultra-Bright X-ray Generation Using Inverse Compton Scattering of Picosecond CO2 Laser Pulses," in this proceeding.

[19] M. Born and E. Wolf, *Principles of Optics*, 6th ed. (Pergamon Press, Oxford, 1986).

[20] Y. Liu, D. Cline, and P. He, *Nucl. Instr. & Meth. in Phys. Res.* A, 424 (2-3), 296 (1999).